Biomech Model Mechanobiol (2009) 8:167–181
DOI 10.1007/s10237-008-0126-1

ORIGINAL PAPER

The micromechanics of fluid–solid interactions during growth in porous soft biological tissue

H. Narayanan · E. M. Arruda · K. Grosh · K. Garikipati

Received: 4 April 2007 / Accepted: 16 April 2008 / Published online: 10 May 2008

Abstract In this paper, we address some modelling issues related to biological growth. Our treatment is based on a formulation for growth that was proposed within the context of mixture theory (J Mech Phys Solids 52:1595–1625, 2004). We aim to make this treatment more appropriate for the physics of porous soft tissues, paying particular attention to the nature of fluid transport, and mechanics of fluid and solid phases. The interactions between transport and mechanics have significant implications for growth and swelling. We also reformulate the governing differential equations for reaction-transport of solutes to represent the incompressibility constraint on the fluid phase of the tissue. This revision enables a straightforward implementation of numerical stabilisation for the advection-dominated limit of these equations. A finite element implementation with operator splitting is used to solve the coupled, non-linear partial differential equations that arise from the theory. We carry out a numerical and analytic study of the convergence of the operator splitting scheme subject to strain- and stress-homogenisation of the mechanics of fluid–solid interactions. A few computations are presented to demonstrate aspects of the physical mechanisms, and the numerical performance of the formulation.

Keywords Mixture theory · Homogenisation · Operator-splitting

1 Introduction

Growth in biological tissue involves the addition or depletion of mass. It often occurs in combination with *remodelling*, which is a change in microstructure, and possibly with *morphogenesis*, which is a change in form in the embryonic state. However, the physics of these processes are quite distinct, and for modelling purposes can, and must, be separated. Our previous work (Garikipati et al. 2004), upon which we now seek to build, drew in some measure from Cowin and Hegedus (1976); Epstein and Maugin (2000), and Taber and Humphrey (2001), and was focused upon a comprehensive account of the coupling between transport and mechanics. The origins of this coupling were traced to the balance equations, kinematics and constitutive relations. A major contribution of that work was the identification and discussion of several driving forces for transport that are thermodynamically consistent in the sense that specification of these relations does not violate the Clausius–Duhem dissipation inequality. The growth part of the deformation gradient was also identified in Garikipati et al. (2004), and treated in a manner similar to Rodriguez et al. (1994). The corresponding numerical treatment via finite element methods was already well-established for non-biological problems (see for example Rao et al. 2000). A treatment related to the notion of evolving natural configurations (proposed in Humphrey and Rajagopal 2002) was later presented in Garikipati et al. (2006).

In this paper, we seek to improve upon our previous work (Garikipati et al. 2004) by refining the models, working out micromechanical details and in one case by eliminating a seemingly misguided term in a constitutive relation. The hoped-for effect is greater physiological relevance to growth in soft biological tissue. We also include one improvement in the mathematical/numerical treatment that enables straightforward numerical stabilisation of the solute mass transport equation in the advection-dominated regime. In order to set the stage for the rest of the paper, we use the next section to summarise relevant results from Garikipati et al. (2004),

H. Narayanan · E. M. Arruda · K. Grosh · K. Garikipati (✉)
Department of Mechanical Engineering, University of Michigan, Ann Arbor, MI 48109-2125, USA
e-mail: krishna@umich.edu

pointing out where the refinements, details or correction need to be introduced. However, we have avoided a full mathematical treatment until the relevant Sects. 3 and 4 of the paper.

2 Background

In this brief section, we highlight the improvements possible or questions left unaddressed in several aspects of the formulation presented in Garikipati et al. (2004).

- For a tissue undergoing finite strain, Garikipati et al. (2004) showed that the transport equations can be formulated in terms of concentrations with respect to either the reference or current (deformed) configuration. However, the fluid–solid interactions and the relevant boundary conditions are most conveniently posed, and understood, in the current configuration (see Sect. 3.1).
- The state of saturation of the tissue was not explicitly considered; however, it is crucial in determining whether the tissue swells or shrinks with infusion/expulsion of fluid (see Sect. 3.2.1).
- The fluid phase was treated as elastic without addressing the question of tensile stress. While such a medium can develop compressive stress without bound, it can develop at most a small tensile stress (Brennen 1995), having implications for the stiffness of the tissue in tension as against compression. Although this also has implications for void formation through cavitation, the ambient pressure in the tissue under normal physiological conditions ensures that this manifests itself only as a reduction in compressive pressure (see Sect. 4.2.1).
- The Fickean diffusion mechanism was considered for fluid transport. This implies the existence of a mixing entropy due to the choice of configurations available to fluid molecules at fixed values of the macroscopic concentration. The relation between fluid saturation and availability of these configurations was left unaddressed, and is now treated in Sect. 4.2.2.
- The acceleration of the solid phase was included as a driving force in the constitutive relation for the flux of other phases. However, acceleration is not frame-invariant and its use in constitutive relations is inappropriate (see Sect. 4.2.3).
- The question of intrinsic incompressibility of fluid and solid phases was not considered. Due to fluid incompressibility, it is common to treat soft biological tissue as either incompressible or nearly incompressible (Fung 1993). At the scale of the pores (assumed to be smaller than the continuum scale of the models in this paper), however, a distinction exists in that the fluid is exactly (or nearly) incompressible, while the porous solid network is not obviously incompressible (see Sect. 4.2.4).
- Chemical solutes in the extra-cellular fluid are advected by fluid flow, and additionally undergo transport under a chemical potential gradient relative to the fluid. In the hyperbolic limit, where advection dominates, spatial instabilities emerge in numerical solutions of these transport equations (Brooks and Hughes 1982; Hughes et al. 1987). Numerical stabilisation of these equations is intimately tied to the mathematical representation of fluid incompressibility, which was not treated in the transport equations (see Sect. 4.2.5).
- The modelling of solid–fluid mechanical coupling carries strong implications for the stiffness of tissue response, the nature of fluid transport, and since nutrients are dissolved in the fluid, ultimately for growth. These issues were not considered. We now address them by drawing upon the limiting cases of strain- and stress-homogenisation between fluid and solid phases. This leads to upper and lower bounds in stiffness and stress gradient-driven fluxes. The corresponding models are presented in Sect. 4.3, and supported by numerical examples in Sect. 5.2.1.

These issues are treated in detail in relevant sections of the paper, which is laid out as follows: balance equations and kinematics are discussed in Sect. 3, constitutive relations for reactions, transport and mechanics in Sect. 4, and numerical examples are presented in Sect. 5. Conclusions are drawn in Sect. 6.

3 Balance equations and kinematics of growth

The growing tissue is an open subset of $\mathbb{R}^3$ and consists of numerous species, of which the following groupings are important for the models: a solid species, consisting of solid *collagen fibrils* and *cells*,[1] denoted by c, an extra-cellular *fluid* species denoted by f and consisting primarily of water, and *solute* species, consisting of precursors to reactions, byproducts, nutrients, and other regulatory chemicals. A generic solute will be denoted by s. In what follows, an arbitrary species will be denoted by ι, where $\iota = \mathrm{c}, \mathrm{f}, \mathrm{s}$.

From fundamental considerations, Garikipati et al. (2004) derived the following balances of mass and momentum, respectively, for an arbitrary species in the reference configuration, Ω_0:

$$\frac{\partial \rho_0^\iota}{\partial t} = \Pi^\iota - \mathrm{DIV}[\boldsymbol{M}^\iota], \ \forall \iota, \quad \text{and} \tag{1}$$

[1] At this point, we do not distinguish the solid species further. This is a good approximation to the physiology of collagenous soft connective tissue, such as tendons, which are relatively acellular and whose dry mass consists of up to 75% collagen (Nordin et al. 2001).

$$\rho_0^\iota \frac{\partial}{\partial t}\left(\boldsymbol{V}+\boldsymbol{V}^\iota\right)=\rho_0^\iota\left(\boldsymbol{g}+\boldsymbol{q}^\iota\right)+\mathrm{DIV}[\boldsymbol{P}^\iota] - \left(\mathrm{GRAD}\left[\boldsymbol{V}+\boldsymbol{V}^\iota\right]\right)\boldsymbol{M}^\iota, \quad \iota=\mathrm{c},\mathrm{f}. \tag{2}$$

Here, ρ_0^ι is the concentration of phase ι, Π^ι is the corresponding mass source term, and $\boldsymbol{M}^\iota$ is the mass flux, all relative to Ω_0. The velocity of the solid collagenous phase is $\boldsymbol{V}$, while $\boldsymbol{V}^\iota$ is the velocity of phase ι relative to the solid collagen. The external body force is $\boldsymbol{g}$, the momentum transferred to phase ι per unit mass is $\boldsymbol{q}^\iota$, and $\boldsymbol{P}^\iota$ is the partial first Piola–Kirchhoff stress of this phase.

A central kinematic assumption was introduced that the pore structure deforms with the collagenous phase. Therefore, the deformation gradient, $\boldsymbol{F}$, is common to c and the fluid-filled pore spaces. This simplifying assumption of strain homogenisation between phases also allowed the imposition of a single momentum balance equation for the composite tissue by summing Eq. (2) over $\iota=\mathrm{c},\mathrm{f}$. It eliminated the need for constitutive prescription of the momentum transfer terms, $\boldsymbol{q}^\mathrm{c}$ and $\boldsymbol{q}^\mathrm{f}$, between the solid collagen and fluid phases, respectively.

3.1 Mass balance in the current configuration, revisited

The initial and boundary value problem of mass transport can be consistently posed in Ω_0, in which case the appropriate Dirichlet boundary condition involves specification of reference concentrations, ρ_0^ι on the boundary. However, it is the current configuration, Ω_t, that is physically accessible for imposition of boundary conditions. Thus, if Dirichlet boundary conditions are imposed, they must be specified for current concentration, $\rho^\iota=\det\boldsymbol{F}^{-1}\rho_0^\iota$. For example, consider mass transport of the fluid with constant ρ^f as the Dirichlet boundary condition, and recall that in the formulation, the shape and size of pores in Ω_t is determined by $\boldsymbol{F}$. If the boundary were in contact with a fluid reservoir, the deforming pores would always be filled with fluid mass that is proportional to the pore volume, and ρ^f would remain constant. In contrast, if the problem were solved on Ω_0 (which is *not* the physically accessible configuration) with constant concentration boundary conditions, this would require specifying $\rho_0^\mathrm{f}=\rho^\mathrm{f}\det\boldsymbol{F}$ on the boundary. This would imply that the physically accessible current concentration, ρ^f, and deformation gradient, $\det\boldsymbol{F}$, need to be specified in a form of "mixed" boundary condition. This is not easily realised, physically. The same arguments can also be made for flux boundary conditions specified on the physically accessible current configuration, Ω_t, and the reference configuration, Ω_0. Since osmotic pressure is determined by relative concentrations, it follows that osmotic pressure boundary conditions also can be posed on the fluid if current solute concentrations, ρ^s, are controlled at the boundaries.

Motivated thus, we use the local form of the balance of mass in the current configuration, Ω_t,

$$\frac{\mathrm{d}\rho^\iota}{\mathrm{d}t}=\pi^\iota-\mathrm{div}[\boldsymbol{m}^\iota]-\rho^\iota\mathrm{div}[\boldsymbol{v}], \quad \forall\,\iota, \tag{3}$$

where π^ι, and $\boldsymbol{m}^\iota$ are the source term and mass flux of phase ι relative to Ω_t. They are related to corresponding reference quantities as $\pi^\iota=\det\boldsymbol{F}^{-1}\Pi^\iota$ and $\boldsymbol{m}^\iota=\det\boldsymbol{F}^{-1}\boldsymbol{F}\boldsymbol{M}^\iota$, with $\boldsymbol{v}$ being the spatial velocity of the solid collagenous phase. The left hand-side in Eq. (3) is the material time derivative relative to the solid, which may be written explicitly as $\frac{\partial}{\partial t}|_X$, implying that the reference position of the solid collagenous skeleton is held fixed.

3.2 Concentration-induced kinematics of growth and swelling

In the stress-free state, biological growth/resorption at a point is caused by an increase/decrease in concentration of the solid collagen, while an increase/decrease in local fluid concentration causes swelling/shrinkage, respectively. This leads to the notion of a *growth or swelling component of the deformation gradient*. One aspect of the coupling between mass transport and mechanics stems from this phenomenon. In the setting of finite strain kinematics, the total deformation gradient, $\boldsymbol{F}$, is decomposed into the growth component of the solid collagen, $\boldsymbol{F}^{\mathrm{g^c}}$, a geometrically necessitated elastic component accompanying growth, $\widetilde{\boldsymbol{F}}^{\mathrm{e^c}}$, and an additional elastic component due to external stress, $\bar{\boldsymbol{F}}^{\mathrm{e^c}}$. We write $\boldsymbol{F}^{\mathrm{e^c}}=\bar{\boldsymbol{F}}^{\mathrm{e^c}}\widetilde{\boldsymbol{F}}^{\mathrm{e^c}}$. This split is analogous to the classical decomposition of multiplicative plasticity (Lee 1969) and is similar to the approach followed in existing literature on biological growth (see e.g., Rodriguez et al. 1994; Klisch et al. 2001; Taber and Humphrey 2001; Ambrosi and Mollica 2002). Having already assumed that the fluid-filled pores also deform with $\boldsymbol{F}$, we identify a component, $\boldsymbol{F}^{\mathrm{e^f}}$, of this total deformation gradient tensor to determine the stress of the fluid, if it is elastic. We also assume a fluid swelling component,[2] $\boldsymbol{F}^{\mathrm{g^f}}$, which we elaborate below, and that $\boldsymbol{F}^{\mathrm{e^f}}\boldsymbol{F}^{\mathrm{g^f}}=\boldsymbol{F}$.

The elastic-growth (-swelling) decomposition is shown in Fig. 1. Assuming that the volume changes associated with growth (swelling) described above are isotropic, a simple form for the growth (swelling) part of the deformation gradient tensor is

$$\boldsymbol{F}^{\mathrm{g}^\iota}=\left(\frac{\rho_0^\iota}{\rho_{0_{\mathrm{ini}}}^\iota}\right)^{\frac{1}{3}}\mathbf{1}, \quad \iota=\mathrm{c},\mathrm{f} \tag{4}$$

[2] Since the kinematical treatment of solid growth and fluid swelling is the same we use the notation $\boldsymbol{F}^{\mathrm{g^f}}$ for the fluid swelling component of the pore deformation gradient, also.

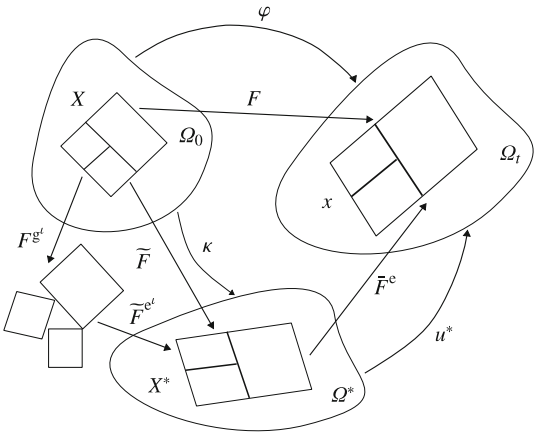

Fig. 1 The kinematics of growth and swelling, for $\iota = \mathrm{c}, \mathrm{f}$, respectively

where $\rho^{\iota}_{0_{\mathrm{ini}}}(\boldsymbol{X})$ is the reference concentration at the initial time, and $\mathbf{1}$ is the second-order isotropic tensor.[3] In the state, $\boldsymbol{F} = \boldsymbol{F}^{\mathrm{g}^{\iota}}$, for $\iota = \mathrm{c}, \mathrm{f}$, the species would be stress free.[4]

3.2.1 *Enhancement of swelling kinematics to account for saturation*

The degree of saturation of the solid phase plays a fundamental role in determining whether the tissue responds to an infusion (expulsion) of fluid by swelling (shrinking). In particular, the isotropic swelling law defined by Eq. (4) has to be generalised to treat the case in which the solid phase is not saturated by fluid.

There exist two possible scenarios: if the tissue is unsaturated in its current configuration, then, on a microscopic scale, it contains unfilled voids. The free volume is available to allow an influx of fluid, and the degree of saturation increases until the tissue is fully saturated. This increase does not cause swelling of the tissue. However, once the tissue is saturated in the current configuration, an increase in the fluid content causes swelling in the stress-free state since there is no free volume for the entering fluid to occupy. This swelling takes place even with an incompressible solid collagenous phase, due to the increase in void volume. The expanding voids remain bounded by the solid collagenous phase which maintains its overall volume. It is this second case that is modelled by (4). It is worth emphasizing that this argument holds for $\boldsymbol{F}^{\mathrm{g}^{\mathrm{f}}}$, which is the local stress-free state of deformation of the fluid-containing pores at a point. The actual deformation gradient, $\boldsymbol{F} = \boldsymbol{F}^{\mathrm{e}^{\mathrm{f}}}\boldsymbol{F}^{\mathrm{g}^{\mathrm{f}}}$, also depends on the elastic part, $\boldsymbol{F}^{\mathrm{e}^{\mathrm{f}}}$, which is determined by the elastic response of the fluid. Under stress, an incompressible fluid will have $\det \boldsymbol{F}^{\mathrm{e}^{\mathrm{f}}} = 1$ and, therefore, a fluid-saturated tissue will swell with fluid influx, $\det \boldsymbol{F} = \det \boldsymbol{F}^{\mathrm{g}^{\mathrm{f}}} > 1$. A compressible fluid may have $\det \boldsymbol{F}^{\mathrm{e}^{\mathrm{f}}} < 1$ allowing $\det \boldsymbol{F} < 1$ even with $\det \boldsymbol{F}^{\mathrm{g}^{\mathrm{f}}} > 1$. Even in this case, however, in the stress-free state there will be swelling.

Therefore, for the fluid-containing pores, the isotropic swelling law can be extended to the unsaturated case by introducing a degree of saturation via the phase volume fraction, ω^{ι}, defined in the current configuration, Ω_t. We have $\omega^{\iota} = \rho^{\iota}/\tilde{\rho}^{\iota}$, where $\tilde{\rho}^{\iota}$ is the intrinsic density in Ω_t and is given by $\tilde{\rho}^{\iota} = \tilde{\rho}^{\iota}_0/\det \boldsymbol{F}$. Note that the intrinsic reference density, $\tilde{\rho}^{\iota}_0$, is a material property. Upon solution of the mass balance Eq. (3) for ρ^{ι}, the species volume fractions, ω^{ι}, can, therefore, be computed in a straightforward fashion. The sum of these volume fractions is our required measure of saturation defined in Ω_t. Also, recognizing that for the dilute solutions obtained with physiologically relevant solute concentrations, the saturation condition is very well approximated by $\omega^{\mathrm{f}} + \omega^{\mathrm{c}} = 1$, we proceed to redefine the fluid swelling-induced component of the pore deformation gradient tensor as follows:

$$\boldsymbol{F}^{\mathrm{g}^{\mathrm{f}}} = \begin{cases} \left(\dfrac{\rho^{\mathrm{f}}_0}{\rho^{\mathrm{f}}_{0_{\mathrm{sat}}}}\right)^{\frac{1}{3}} \mathbf{1}, & \omega^{\mathrm{f}} + \omega^{\mathrm{c}} = 1 \\ \mathbf{1}, & \text{otherwise.} \end{cases} \tag{5}$$

In (5) $\rho^{\mathrm{f}}_{0_{\mathrm{sat}}}$ is the reference concentration value at which the tissue attains saturation in the current configuration.

With this redefinition of $\boldsymbol{F}^{\mathrm{g}^{\mathrm{f}}}$ it is implicit that $\omega^{\mathrm{f}} + \omega^{\mathrm{c}} > 1$ is non-physical. Saturation holds in the sense that $\omega^{\mathrm{f}} + \omega^{\mathrm{c}} = 1$. It has been common in the soft tissue literature to assume that, under normal physiological conditions, soft tissues are fully saturated by the fluid and Eq. (4) is appropriate for $\iota = \mathrm{f}$. However, this treatment of saturation and swelling induced by the fluid phase is necessary background for Sect. 4.2.1 where we discuss the response of the fluid phase under tension. This treatment also holds relevance for partial drying, which ex vivo or in vitro tissue may be subject to under certain laboratory conditions, and is central to the mechanics of drained porous media other than biological tissue, most prominently, soils.

[3] This choice is only the simplest possible. Given the highly directional micro-structure and mechanical properties of many tissues, it seems likely that anisotropic growth is actually more common. Wolff's law for bone growth is one example. This is a topic of ongoing investigation, and one that we will report on in greater detail in a future communication.

[4] For completeness, we note that the velocity of the fluid relative to the solid collagen is $\boldsymbol{V}^{\mathrm{f}} = \rho^{\mathrm{f}^{-1}}\boldsymbol{m}^{\mathrm{f}}$ (see Garikipati et al. 2004), and the total fluid velocity satisfies $\partial \boldsymbol{V}^{\mathrm{f}}_{\mathrm{tot}}/\partial \boldsymbol{X} = \boldsymbol{F}^{\mathrm{e}^{\mathrm{f}}}\boldsymbol{F}^{\mathrm{g}^{\mathrm{f}}} + \partial \boldsymbol{V}^{\mathrm{f}}/\partial \boldsymbol{X}$.

4 Constitutive relations: review and enhancements

4.1 Constitutive relations reviewed

4.1.1 An anisotropic network model based on entropic elasticity

In order to enable the discussion of constitutive relations we summarise the material model adopted in Garikipati et al. (2004). It is applicable to collagen-rich soft tissue with strong orthotropy, such as tendons and ligaments. The strain energy density has been obtained from hierarchical multi-scale considerations based upon an entropic elasticity-based worm-like chain (WLC) model (Kratky and Porod 1949). The central parameters of this model are the chain's contour length, L, and persistence length, A. The latter is a measure of its stiffness and given by $A = \chi/k\theta$, where χ is the bending rigidity, k is Boltzmann's constant and θ is the temperature.

To model a collagen network structure, the WLC model has been embedded as a single constituent chain of an eight-chain model (Bischoff et al. 2002a,b), depicted in Fig. 2. Homogenisation via averaging then leads to a continuum Helmholtz free energy function, $\hat{\psi}^{\mathrm{c}}$:[5]

$$\begin{aligned}\rho_0^{\mathrm{c}}\hat{\psi}^{\mathrm{c}}\left(\boldsymbol{F}^{\mathrm{e^c}},\rho_0^{\mathrm{c}}\right) &= \frac{Nk\theta}{4A}\left(\frac{r^2}{2L}+\frac{L}{4(1-r/L)}-\frac{r}{4}\right)\\ &\quad+\frac{\gamma}{\beta}\left(J^{\mathrm{e^c}-2\beta}-1\right)+\gamma\mathbf{1}:(\boldsymbol{C}^{\mathrm{e^c}}-\mathbf{1})\\ &\quad-\frac{Nk\theta}{4\sqrt{2L/A}}\\ &\quad\times\left(\sqrt{\frac{2A}{L}}+\frac{1}{4(1-\sqrt{2A/L})}-\frac{1}{4}\right)Z,\\ Z &= \log\left(\lambda_1^{\mathrm{e}a^2}\lambda_2^{\mathrm{e}b^2}\lambda_3^{\mathrm{e}c^2}\right).\end{aligned}\tag{6}$$

Here, N is the density of chains, and a, b and c are lengths of the unit cell sides aligned with the principal stretch directions. The material model is isotropic only if $a = b = c$.

The elastic stretches along the unit cell axes are, respectively, denoted by λ_1^{e}, λ_2^{e} and λ_3^{e}, $\boldsymbol{C}^{\mathrm{e^c}} = \boldsymbol{F}^{\mathrm{e^c}^{\mathrm{T}}}\boldsymbol{F}^{\mathrm{e^c}}$ is the elastic right Cauchy–Green tensor of collagen. The factors γ and β control the bulk compressibility of the model. The end to end chain length is given by $r = \frac{1}{2}\sqrt{a^2\lambda_1^{\mathrm{e}^2}+b^2\lambda_2^{\mathrm{e}^2}+c^2\lambda_3^{\mathrm{e}^2}}$, where $\lambda_I^{\mathrm{e}} = \sqrt{\boldsymbol{N}_I\cdot\boldsymbol{C}^{\mathrm{e^c}}\boldsymbol{N}_I}$, and $\boldsymbol{N}_I$, $I = 1, 2, 3$ are the unit vectors along the three unit cell axes, respectively. The form in which the physical lengths A, L, a, b and c appear in (6) makes clear that they can all be nondimensionalised with respect to any chosen length scale. It is only their relative lengths that affect the response. This nondimensionalization has been used in Table 1. In our numerical simulations that appear below in Sect. 5, the values used for the parameters introduced in (6) are based on those in Kuhl et al. (2005).

[5] Under the isothermal conditions assumed here, $\hat{\psi}^{\mathrm{c}}$ is independent of θ in the strain energy. Accordingly, we have the parametrisation $\psi^{\mathrm{c}} = \hat{\psi}^{\mathrm{c}}(\boldsymbol{F}^{\mathrm{e^c}}, \rho_0^{\mathrm{c}})$.

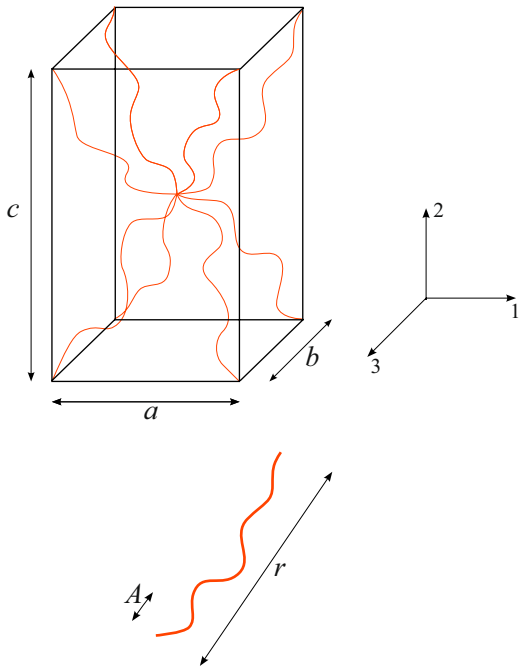

Fig. 2 The eight-chain model incorporating worm-like chains

Table 1 Material parameters used in the analysis

Parameter (symbol)	Value	Units
Chain density (N)	7×10^{21}	m^{-3}
Temperature (θ)	310.6	K
Persistence length (A)	2.10	–
Fully stretched length (L)	2.125	–
Unit cell axes (a, b, c)	1.95, 1.95, 2.43	–
Bulk compressibility factors (γ, β)	1,000, 4.5	KPa, –
Fluid bulk modulus (κ^{f})	1	GPa
Fluid mobility tensor ($D_{ij}^{\mathrm{f}} = D^{\mathrm{f}}\delta_{ij}$)	1×10^{-14}	s
Fibroblast concentration (ρ_{cell})	0.2	$\mathrm{kg.m}^{-3}$
Max. reaction rate ($k_{\max} = 5$)	5	s^{-1}
Max. solute concentration ($\rho_{\mathrm{m}}^{\mathrm{s}}$)	0.2	$\mathrm{kg\ m}^{-3}$
Solute diffusivity ($\boldsymbol{D}^{\mathrm{s}}$)	1×10^{-9}	$\mathrm{m}^{-2}\mathrm{s}$

4.1.2 A nearly incompressible ideal fluid

The fluid phase is treated as inviscid, elastic and nearly incompressible. The partial Cauchy stress in the fluid is

$$\boldsymbol{\sigma}^{\mathrm{f}} = \det(\boldsymbol{F}^{\mathrm{e^f}})^{-1}\boldsymbol{P}^{\mathrm{f}}\boldsymbol{F}^{\mathrm{e^f T}} = h(\rho^{\mathrm{f}})\mathbf{1},\tag{7}$$

where a large value of $h'(\rho^{\mathrm{f}})$ ensures near-incompressibility. The following simple quadratic model is used:

$$h(\rho^{\mathrm{f}}) = \frac{1}{2}\kappa^{\mathrm{f}}\left(\frac{\rho^{\mathrm{f}}_{0_{\mathrm{ini}}}}{\rho^{\mathrm{f}}} - 1\right)^2, \tag{8}$$

where κ^{f} is the fluid bulk modulus.

4.1.3 Constitutive relations for fluid flux

From Garikipati et al. (2004), the constitutive relation for the flux of extra-cellular fluid relative to collagen in the reference configuration takes the following form,

$$\boldsymbol{M}^{\mathrm{f}} = \boldsymbol{D}^{\mathrm{f}}\left(\rho^{\mathrm{f}}_0 \boldsymbol{F}^{\mathrm{T}}\boldsymbol{g} + \boldsymbol{F}^{\mathrm{T}}\mathrm{DIV}\left[\boldsymbol{P}^{\mathrm{f}}\right] - \rho^{\mathrm{f}}_0 \mathrm{GRAD}\mu^{\mathrm{f}}\right), \tag{9}$$

where $\boldsymbol{D}^{\mathrm{f}}$ is the positive semi-definite mobility of the fluid, and μ^{f} is the chemical potential, consisting of energetic and mixing entropic contributions.

4.1.4 Transport of solute species

The dissolved solute species undergo long range transport primarily by a combination of advection by the fluid and diffusion relative to the fluid. This motivates an additional velocity split of the form $\boldsymbol{V}^{\mathrm{s}} = \widetilde{\boldsymbol{V}}^{\mathrm{s}} + \boldsymbol{V}^{\mathrm{f}}$, where $\widetilde{\boldsymbol{V}}^{\mathrm{s}}$ denotes the velocity of the solute relative to the fluid. The constitutive relation for the corresponding flux, denoted by $\widetilde{\boldsymbol{M}}^{\mathrm{s}}$, has the following form:

$$\widetilde{\boldsymbol{M}}^{\mathrm{s}} = \boldsymbol{D}^{\mathrm{s}}\left(-\rho^{\mathrm{s}}_0 \mathrm{GRAD}\mu^{\mathrm{s}}\right), \tag{10}$$

where $\boldsymbol{D}^{\mathrm{s}}$ is the positive semi-definite mobility of the solute relative to the fluid and μ^{s} is the chemical potential. There are no stress-dependent contributions to $\widetilde{\boldsymbol{M}}^{\mathrm{s}}$.

4.1.5 Source terms

There exists a large body of literature (Cowin and Hegedus 1976; Epstein and Maugin 2000; Ambrosi and Mollica 2002), that addresses growth in biological tissue mainly based upon a single species undergoing transport and production/annihilation. However, growth actually depends on cascades of complex biochemical reactions involving several species. In Garikipati et al. (2004), chemical reactions between species were modelled by using first order chemical kinetics for Π^{c}. In this paper, we also consider the classical Michaelis–Menten enzyme kinetics (e.g., Sengers et al. 2004), which involves a two-step reaction with the collagen and solute production terms given by

$$\Pi^{\mathrm{s}} = \frac{-(k_{\max}\rho^{\mathrm{s}})}{(\rho^{\mathrm{s}}_m + \rho^{\mathrm{s}})}\rho_{\mathrm{cell}}, \quad \Pi^{\mathrm{c}} = -\Pi^{\mathrm{s}}, \tag{11}$$

where ρ_{cell} is the concentration of fibroblasts, $k_{\max}$ is the maximum value of the solute production reaction rate constant, and ρ^{s}_m is half the solute concentration corresponding to $k_{\max}$. For details on the chemistry modelled by the Michaelis–Menten model see Bromberg and Dill (2002).

4.2 Constitutive models enhanced

4.2.1 Response of the fluid in tension; cavitation

The response of the fluid, as defined by Eq. (7), does not distinguish between tension and compression, i.e., whether $\det(\boldsymbol{F}^{\mathrm{e^f}}) \gtrless 1$. Being nearly incompressible, the fluid can develop compressive hydrostatic stress without bound—a case that is modelled accurately. However, the fluid can develop at most a small tensile hydrostatic stress (Brennen 1995),[6] and the tensile stiffness of the composite tissue is mainly from the collagen phase.

We modify the fluid stress response to preclude all tensile load by limiting $\det(\boldsymbol{F}^{\mathrm{e^f}}) \leq 1$. We first introduce an additional component to the relation between deformation of the pore space, given by $\boldsymbol{F}$, the fluid stress-determining tensor, $\boldsymbol{F}^{\mathrm{e^f}}$ and the swelling tensor for the fluid, $\boldsymbol{F}^{\mathrm{g^f}}$. Consider the cavitation (void forming) tensor, $\boldsymbol{F}^{\mathrm{v}}$, defined by

$$\boldsymbol{F}^{\mathrm{e^f}}\boldsymbol{F}^{\mathrm{g^f}}\boldsymbol{F}^{\mathrm{v}} = \boldsymbol{F}. \tag{12}$$

We restrict the formulation to include only saturated current configurations at $t = 0$. Following Sect. 3.2.1, we have $\omega^{\mathrm{f}} + \omega^{\mathrm{c}} = 1$ at $t = 0$, the saturation condition in Ω_t when solutes are at low concentrations. At times $t > 0$ Eq. (5) holds for $\boldsymbol{F}^{\mathrm{g^f}}$. If $\det[\boldsymbol{F}(\boldsymbol{F}^{\mathrm{g^f}})^{-1}] \leq 1$ we set $\boldsymbol{F}^{\mathrm{e^f}} = \boldsymbol{F}(\boldsymbol{F}^{\mathrm{g^f}})^{-1}$ and $\boldsymbol{F}^{\mathrm{v}} = \boldsymbol{1}$ for no cavitation. Otherwise, since $\det[\boldsymbol{F}(\boldsymbol{F}^{\mathrm{g^f}})^{-1}] > 1$, we specify $\boldsymbol{F}^{\mathrm{e^f}} = \det[\boldsymbol{F}(\boldsymbol{F}^{\mathrm{g^f}})^{-1}]^{-1/3}\boldsymbol{F}(\boldsymbol{F}^{\mathrm{g^f}})^{-1}$ thus restricting $\boldsymbol{F}^{\mathrm{e^f}}$ to be unimodular and allow cavitation by writing $\boldsymbol{F}^{\mathrm{v}} = \boldsymbol{F}(\boldsymbol{F}^{\mathrm{e^f}}\boldsymbol{F}^{\mathrm{g^f}})^{-1}$. These conditional relations are summarised as

$$\boldsymbol{F}^{\mathrm{e^f}} = \begin{cases} \boldsymbol{F}(\boldsymbol{F}^{\mathrm{g^f}})^{-1} \text{ and } \boldsymbol{F}^{\mathrm{v}} = \boldsymbol{1}, & \text{if } \det[\boldsymbol{F}(\boldsymbol{F}^{\mathrm{g^f}})^{-1}] \leq 1 \\ \det[\boldsymbol{F}(\boldsymbol{F}^{\mathrm{g^f}})^{-1}]^{-1/3}\boldsymbol{F}(\boldsymbol{F}^{\mathrm{g^f}})^{-1}, & \\ \quad \text{and } \boldsymbol{F}^{\mathrm{v}} = \boldsymbol{F}(\boldsymbol{F}^{\mathrm{e^f}}\boldsymbol{F}^{\mathrm{g^f}})^{-1} & \text{otherwise.} \end{cases} \tag{13}$$

4.2.2 Saturation and Fickean diffusion of the fluid

Only when pores are unsaturated with fluid are there multiple configurations available to the fluid molecules at a fixed fluid concentration. This leads to a non-zero mixing entropy. In contrast, under conditions of fluid saturation, there is a single available configuration, resulting in zero mixing entropy. Consequently, Fickean diffusion, which arises from the gradient of mixing entropy can exist only in the unsaturated

[6] Where, we are referring to the fluid being subject to net tension, not a reduction in fluid compressive stress from reference ambient pressure.

case. However, even a saturated pore structure can demonstrate concentration gradient-dependent mass transport: the fluid stress depends on fluid concentration [see Eq. (7)], and fluid stress gradient-driven flux appears as a concentration gradient-driven flux.

The saturation dependence of Fickean diffusion is modelled by using the measure of saturation introduced in Sect. 3.2.1. We now write the chemical potential as

$$\begin{aligned} \mu^{\mathrm{f}} &= e^{\mathrm{f}} - \theta\eta^{\mathrm{f}}, \\ \eta^{\mathrm{f}} &\to 0, \quad \text{as } \omega^{\mathrm{f}} + \omega^{\mathrm{c}} \to 1, \end{aligned} \tag{14}$$

where e^{f}, η^{f} and θ are, respectively, the mass-specific internal energy and entropy, and the temperature, respectively. It is again important to note that under physiological conditions, soft tissues are fully saturated by fluid, and it is appropriate to set $\mu^{\mathrm{f}} = e^{\mathrm{f}}$.

4.2.3 Frame invariance and the contribution from acceleration

In our earlier treatment (Garikipati et al. 2004), the constitutive relation for the fluid flux had a driving force contribution arising from the acceleration of the solid phase, $-\rho_0^{\mathrm{f}} \boldsymbol{F}^{\mathrm{T}} \frac{\partial \boldsymbol{V}}{\partial t}$. This term, being motivated by the reduced dissipation inequality, does not violate the Second Law and supports an intuitive understanding that the acceleration of the solid skeleton in one direction must result in an inertial driving force on the fluid in the opposite direction. However, as defined, this acceleration is obtained by the time differentiation of kinematic quantities,[7] and does not transform in a frame-indifferent manner. Unlike the superficially similar term arising from the gravity vector,[8] the acceleration term presents an improper dependence on the frame of the observer. Thus, its use in constitutive relations is inappropriate, and the term has been dropped in Eq. (9).

4.2.4 Incompressible fluid in a porous solid

Upon incorporation of the additional velocity split, $\boldsymbol{V}^{\mathrm{s}} = \widetilde{\boldsymbol{V}}^{\mathrm{s}} + \boldsymbol{V}^{\mathrm{f}}$, described in Sect. 4.1.1.4, the resulting mass transport Eq. (3) for the solute species is

$$\frac{\mathrm{d}\rho^{\mathrm{s}}}{\mathrm{d}t} = \pi^{\mathrm{s}} - \mathrm{div}\left[\widetilde{\boldsymbol{m}^{\mathrm{s}}} + \frac{\rho^{\mathrm{s}}}{\rho^{\mathrm{f}}}\boldsymbol{m}^{\mathrm{f}}\right] - \rho^{\mathrm{s}}\mathrm{div}[\boldsymbol{v}]. \tag{15}$$

[7] And not in terms of acceleration *relative to fixed stars* (Truesdell and Noll 1965, p. 43).

[8] Where every observer has an implicit knowledge of the directionality of the field relative to a fixed frame, allowing it to transform objectively. Specifically, under a time-dependent rigid body motion imposed on the current configuration carrying $\boldsymbol{x}$ to $\boldsymbol{x}^+ = \boldsymbol{c}(t) + \boldsymbol{Q}(t)\boldsymbol{x}$, where $\boldsymbol{c}(t) \in \mathbb{R}^3$ and $\boldsymbol{Q}(t) \in \mathrm{SO}(3)$, it is understood that the acceleration due to gravity in the transformed frame is $\boldsymbol{g}^+ = \boldsymbol{Q}^{\mathrm{T}}\boldsymbol{g}$ and is, therefore, frame-invariant. However, the acceleration transforms as $\boldsymbol{a}^+ = \ddot{\boldsymbol{c}} + 2\dot{\boldsymbol{Q}}\boldsymbol{v} + \ddot{\boldsymbol{Q}}\boldsymbol{x} + \boldsymbol{Q}\boldsymbol{a}$, and is, therefore, not frame-invariant.

In the hyperbolic limit, where advection dominates, spatial oscillations emerge in numerical solutions of this equation (Brooks and Hughes 1982; Hughes et al. 1987). Furthermore, (15) is not in standard advection–diffusion form, and, therefore, is not amenable to the application of standard stabilisation techniques (Hughes et al. 1987). In part, this is because although the near incompressibility of the fluid phase is embedded in the balance of linear momentum via the fluid stress, it has not yet been explicitly incorporated into the transport equations. This drawback is eliminated in this section by imposition of the limiting case of fluid incompressibility. The implications for the solute mass transport equation are derived, including a crucial simplification that allows straightforward numerical stabilisation of Eq. (15).

Setting the fluid source term $\pi^{\mathrm{f}} = 0$ in Eq. (3) leads to the following balance of mass in the current configuration:

$$\frac{\mathrm{d}\rho^{\mathrm{f}}}{\mathrm{d}t} = -\mathrm{div}\left[\boldsymbol{m}^{\mathrm{f}}\right] - \rho^{\mathrm{f}}\mathrm{div}\left[\boldsymbol{v}\right]. \tag{16}$$

In order to impose the incompressibility of the fluid, we first denote by $\rho^{\mathrm{f}}_{0_{\mathrm{ini}}}$ the *initial* value of the fluid reference concentration. Recall that the fluid concentration with respect to the reference configuration evolves in time; $\rho_0^{\mathrm{f}} = \rho_0^{\mathrm{f}}(\boldsymbol{X}, t)$. Therefore, we can precisely, and non-trivially, define $\rho^{\mathrm{f}}_{0_{\mathrm{ini}}}(\boldsymbol{X})$

$$\begin{aligned} \rho_0^{\mathrm{f}}(\boldsymbol{X}, 0) =: \rho^{\mathrm{f}}_{0_{\mathrm{ini}}}(\boldsymbol{X}) &= \rho^{\mathrm{f}}_{\mathrm{ini}}(\boldsymbol{x} \circ \boldsymbol{\varphi}) J(\boldsymbol{X}, t) \\ &= \frac{\rho^{\mathrm{f}}(\boldsymbol{x} \circ \boldsymbol{\varphi}, t)}{J^{\mathrm{fg}}(\boldsymbol{X}, t)} J(\boldsymbol{X}, t) \\ &= \rho^{\mathrm{f}}(\boldsymbol{x} \circ \boldsymbol{\varphi}, t) \underbrace{J^{\mathrm{fe}}}_{\approx 1 \;\forall\, t}(\boldsymbol{X}, t). \end{aligned} \tag{17}$$

In (17), $J := \det(\boldsymbol{F})$ and $J^{\mathrm{fg}} := \det(\boldsymbol{F}^{\mathrm{gf}})$. The quantity $\rho^{\mathrm{f}}_{\mathrm{ini}}$ is defined by the right hand-sides of the first and second lines of (17). To follow the argument, consider, momentarily, a *compressible* fluid. If the current concentration, ρ^{f}, changes due to elastic deformation of the fluid and by transport, then $\rho^{\mathrm{f}}_{\mathrm{ini}}$ as defined is not a physically realised fluid concentration. It bears a purely mathematical relation to the current concentration, ρ^{f}, since the latter quantity represents the effect of deformation of a tissue point as well as change in mass due to transport at that point. If the contribution due to mass change at a point is scaled out of ρ^{f} the quotient is identical to the result of dividing $\rho^{\mathrm{f}}_{0_{\mathrm{ini}}}$ by the deformation only. This is expressed in the relation between the right hand-sides of the second and third lines of (17). The elastic component of fluid volume change in a pore is $J^{\mathrm{fe}} := \det(\boldsymbol{F}^{\mathrm{ef}})$, which appears in the third line of (17) via the preceding arguments. Clearly then, for a fluid demonstrating near intrinsic incompressibility (i.e., the true density is nearly constant), we have $J^{\mathrm{fe}} \approx 1$ as indicated. Equation (17), therefore, shows that for a nearly incompressible fluid occupying the pores of a tissue, if we further assume that the pore structure deforms as

the solid collagenous skeleton, $\rho_0^{\mathrm{f}}(\boldsymbol{X},0) \approx \rho^{\mathrm{f}}(\boldsymbol{x}\circ\boldsymbol{\varphi},t)$. The fluid concentration as measured in the current configuration is approximately constant in space and time. This allows us to write,

$$\frac{\partial}{\partial t}\left(\rho_{0_{\mathrm{ini}}}^{\mathrm{f}}(\boldsymbol{X})\right) \equiv 0 \Rightarrow \frac{\partial}{\partial t}\left(\rho^{\mathrm{f}}(\boldsymbol{x}\circ\boldsymbol{\varphi},t)\right)\Big|_{\boldsymbol{X}} = 0, \tag{18}$$

which is the hidden implication of our assumption of a homogeneous deformation between phases. This leads to $\frac{\mathrm{d}\rho^{\mathrm{f}}}{\mathrm{d}t} = 0$.[9] We, therefore, proceed to treat our fluid mass transport at steady state. Rewriting the flux $\boldsymbol{m}^{\mathrm{f}}$ from Eq. (16) as the product $\rho^{\mathrm{f}}\boldsymbol{v}^{\mathrm{f}}$ and using the result derived above,

$$\begin{aligned} 0 &= \left.\frac{\partial \rho^{\mathrm{f}}}{\partial t}\right|_{\boldsymbol{X}} \\ &= -\mathrm{div}\left[\rho^{\mathrm{f}}\boldsymbol{v}^{\mathrm{f}}\right] - \rho^{\mathrm{f}}\mathrm{div}\left[\boldsymbol{v}\right]. \end{aligned} \tag{19}$$

Returning to (15) with this result,

$$\begin{aligned} \frac{\mathrm{d}\rho^{\mathrm{s}}}{\mathrm{d}t} &= \pi^{\mathrm{s}} - \mathrm{div}\left[\widetilde{\boldsymbol{m}}^{\mathrm{s}} + \frac{\rho^{\mathrm{s}}}{\rho^{\mathrm{f}}}\boldsymbol{m}^{\mathrm{f}}\right] - \rho^{\mathrm{s}}\mathrm{div}[\boldsymbol{v}] \\ &= \frac{\rho^{\mathrm{s}}}{\rho^{\mathrm{f}}}\underbrace{\left(-\mathrm{div}\left[\rho^{\mathrm{f}}\boldsymbol{v}^{f}\right] - \rho^{\mathrm{f}}\mathrm{div}[\boldsymbol{v}]\right)}_{0} \\ &\quad + \pi^{\mathrm{s}} - \mathrm{div}\left[\widetilde{\boldsymbol{m}}^{\mathrm{s}}\right] - \boldsymbol{m}^{\mathrm{f}}\cdot\mathrm{grad}\left[\frac{\rho^{\mathrm{s}}}{\rho^{\mathrm{f}}}\right]. \end{aligned} \tag{20}$$

Thus, using the incompressibility condition (19), we get the simplified form of the balance of mass for an arbitrary solute species, s,

$$\begin{aligned} \frac{\mathrm{d}\rho^{\mathrm{s}}}{\mathrm{d}t} &= \pi^{\mathrm{s}} - \mathrm{div}\left[\widetilde{\boldsymbol{m}}^{\mathrm{s}}\right] - \frac{\boldsymbol{m}^{\mathrm{f}}\cdot\mathrm{grad}\left[\rho^{\mathrm{s}}\right]}{\rho^{\mathrm{f}}} \\ &\quad + \frac{\rho^{\mathrm{s}}\boldsymbol{m}^{\mathrm{f}}\cdot\mathrm{grad}\left[\rho^{\mathrm{f}}\right]}{\rho^{f^2}}. \end{aligned} \tag{21}$$

Using the pushed-forward form of (10), this is now in standard advection–diffusion form,

$$\begin{aligned} &\frac{\mathrm{d}\rho^{\mathrm{s}}}{\mathrm{d}t} - \underbrace{\mathrm{div}\left[\bar{\boldsymbol{D}}^{\mathrm{s}}\mathrm{grad}\left[\rho^{\mathrm{s}}\right]\right]}_{\text{Diffusion term}} - \underbrace{\pi^{\mathrm{s}}}_{\text{Source term}} \\ &\quad = \underbrace{-\frac{\boldsymbol{m}^{\mathrm{f}}\cdot\mathrm{grad}\left[\rho^{\mathrm{s}}\right]}{\rho^{\mathrm{f}}}}_{\text{Advection term}} + \underbrace{\frac{\rho^{\mathrm{s}}\boldsymbol{m}^{\mathrm{f}}\cdot\mathrm{grad}\left[\rho^{\mathrm{f}}\right]}{\rho^{\mathrm{f}^2}}}_{\text{Additional, }\rho^{\mathrm{s}}\text{-dependent source term}}, \end{aligned} \tag{22}$$

where $\bar{\boldsymbol{D}}^{\mathrm{s}}$ is a positive semi-definite diffusivity, $\boldsymbol{m}^{\mathrm{f}}/\rho^{\mathrm{f}}$ is the advective velocity, and π^{s} is the volumetric source term. This form is well suited for stabilisation schemes such as the streamline upwind Petrov–Galerkin (SUPG) method (Hughes et al. 1987), described briefly below, which limit spatial oscillations otherwise observed when the element Peclet number is large.

[9] It results in a very large pressure gradient driven flux due to incompressibility.

4.2.5 Stabilisation of the simplified solute transport equation

In weak form, the SUPG-stabilised method for Eq. (22) is

$$\begin{aligned} &\int_{\Omega} w^{\mathrm{h}}\left(\frac{\mathrm{d}\rho^{\mathrm{s}^{\mathrm{h}}}}{\mathrm{d}t} + \boldsymbol{m}^{\mathrm{f}}\cdot\mathrm{grad}\left[\frac{\rho^{\mathrm{s}^{\mathrm{h}}}}{\rho^{\mathrm{f}}}\right]\right)\mathrm{d}\Omega \\ &\quad + \int_{\Omega}\left(\mathrm{grad}\left[w^{\mathrm{h}}\right]\cdot\bar{\boldsymbol{D}}^{\mathrm{s}}\mathrm{grad}\left[\rho^{\mathrm{s}^{\mathrm{h}}}\right]\right)\mathrm{d}\Omega \\ &\quad + \sum_{e=1}^{n_{el}}\int_{\Omega_e}\tau\frac{\boldsymbol{m}^{\mathrm{f}}}{\rho^{\mathrm{f}}}\cdot\mathrm{grad}\left[w^{\mathrm{h}}\right] \\ &\quad \times\left(\frac{\mathrm{d}\rho^{\mathrm{s}^{\mathrm{h}}}}{\mathrm{d}t} + \boldsymbol{m}^{\mathrm{f}}\cdot\mathrm{grad}\left[\frac{\rho^{\mathrm{s}^{\mathrm{h}}}}{\rho^{\mathrm{f}}}\right]\right)\mathrm{d}\Omega \\ &\quad - \sum_{e=1}^{n_{el}}\int_{\Omega_e}\tau\frac{\boldsymbol{m}^{\mathrm{f}}}{\rho^{\mathrm{f}}}\cdot\mathrm{grad}\left[w^{\mathrm{h}}\right]\left(\mathrm{div}\left[\bar{\boldsymbol{D}}^{\mathrm{s}}\mathrm{grad}\left[\rho^{\mathrm{s}^{\mathrm{h}}}\right]\right]\right)\mathrm{d}\Omega \\ &= \int_{\Omega} w^{\mathrm{h}}\pi^{\mathrm{s}}\,\mathrm{d}\Omega + \int_{\Gamma_{\mathrm{h}}} w^{\mathrm{h}}h\,\mathrm{d}\Gamma \\ &\quad + \sum_{e=1}^{n_{el}}\int_{\Omega_e}\tau\frac{\boldsymbol{m}^{\mathrm{f}}}{\rho^{\mathrm{f}}}\cdot\mathrm{grad}\left[w^{\mathrm{h}}\right]\pi^{\mathrm{s}}\,\mathrm{d}\Omega, \end{aligned} \tag{23}$$

where quantities with the superscript h represent finite-dimensional approximations of infinite-dimensional field variables, Γ_{h} is the Neumann boundary, and this equation introduces a numerical stabilisation parameter τ, which we have calculated from the L_2 norms of element level matrices, as described in Tezduyar and Sathe (2003).

The formulation with the enhancements discussed in Sects. 3.1, 3.2, and 4.2.1–4.2.5 has been used to solve a numerical example in Sect. 5.1. The complexity of the formulation merits a consideration of its numerical stability, which is the aim of Sect. 5.1. Subsequent numerical examples are focused on further studying the origins of the convergence characteristics, resulting from the models, and using this study as a basis for a computation demonstrating growth and swelling.

4.3 Strain- and stress-homogenisation of solid–fluid interaction

The strain homogenisation assumption was introduced in Sect. 3 and has underlain the formulation up to this point. It is well-known from the theory of composite materials that this assumption results in the upper bound for the effective stiffness of the tissue—the Voigt model (Milton 2002).

Therefore, the stress gradient-driven fluid flux, whose derivation was discussed in detail in Garikipati et al. (2004), also attains its upper bound. We refer to this formulation as the *upper bound model*. In Sect. 5.2.1, we present a numerical example demonstrative of such a fluid flux field (Fig. 6a).

In order to identify the range over which the fluid flux magnitude can vary, we now introduce the *lower bound model* on effective stiffness of the tissue and, consequently, the magnitude of the stress gradient-driven fluid flux. For this lower bound, we replace the earlier strain homogenisation requirement with a stress homogenisation requirement, viz., equating the hydrostatic stress of the solid phase and the fluid pressure in the current configuration:

$$p^{\mathrm{f}} = \frac{1}{3}\mathrm{tr}[\boldsymbol{\sigma}^{\mathrm{c}}], \tag{24}$$

where p^{f} is the fluid pressure in the current configuration, $\mathrm{tr}[\bullet]$ is the trace operator, and $\boldsymbol{\sigma}^{c} = \frac{1}{\det \boldsymbol{F}^{\mathrm{c}}} \boldsymbol{P}^{\mathrm{c}} \boldsymbol{F}^{\mathrm{c}^{\mathrm{T}}}$ is the Cauchy stress of the solid. The motivation for this model comes from Cauchy's theorem that two bodies in contact and in mechanical equilibrium have equal and opposite traction at the contact surface. We have extended this idea to equality of the traces of their respective Cauchy stress tensors. The Cauchy stress of an ideal fluid can be defined from its pressure as $\boldsymbol{\sigma}^{\mathrm{f}} = p^{\mathrm{f}}\mathbf{1}$. The theory of composite materials confirms that such stress homogenisation leads to lower bounds on the effective stiffness—the Reuss model. Section 5.2.1 shows the fluid flux field (Fig. 6b) when the lower bound model underlies fluid–solid interactions, and presents a discussion of the physical and numerical implications of the two bounds.

5 Numerical examples

The theory presented in the preceding sections results in a system of non-linear, coupled partial differential equations. A finite element formulation employing a staggered scheme based upon operator splits (Armero 1999; Garikipati and Rao 2001) has been implemented in the nonlinear finite element code FEAP (Taylor 1999) to solve the coupled problem. Each (nonlinear, in general) partial differential equation is solved for the corresponding primitive variable while holding the primitive variables of the other equations fixed. A sequence in which each equation is solved exactly once by this staggered scheme constitutes a single pass of the algorithm. Several passes are performed until the resulting fields satisfy the differential equations within a specified numerical tolerance, forming a self-consistent solution.

The balance of linear momentum that we solve is (2) summed for $\iota = \mathrm{c}, \mathrm{f}$ as explained in the text following that equation. The absence of significant acceleration in the problems under consideration allows us to solve the balance of linear momentum quasi-statically. The fluid mass balance equation is solved in the current configuration, i.e. (3) for $\iota = \mathrm{f}$, but mass balance for the solid collagenous phase is solved in the reference configuration, i.e. (1) for $\iota = \mathrm{c}$. Mass balance for the solute is also solved in the current configuration, but using the stabilised scheme in weak form (23). The backward Euler algorithm is used for all mass transport equations. The constitutive relation for the solid collagen follows (6). The constitutive relation for the fluid stress follows (7) and (8). Nonlinear projection methods (Simo et al. 1985) are used to treat the near-incompressibility imposed by the fluid. Mixed methods, as described in Garikipati and Rao (2001), are used for stress gradient-driven fluxes. The tissue is modelled as being fluid saturated in Ω_t at $t = 0$, i.e. (5_1) holds with $\rho^{\mathrm{f}}_{0_{\mathrm{sat}}} = \rho^{\mathrm{f}}_{0_{\mathrm{ini}}}$. However, the tissue is allowed to become unsaturated in Ω_t for $t > 0$ due to void formation. Then, the conditions set out in (13) apply. The chemical potential is then given by (14). The numerical values of parameters[10] that have been used appear in Table 1.

The following numerical examples aim to demonstrate the mathematical formulation and certain aspects of the coupled physical phenomena as the tissue swells and grows. The model geometry, based on engineered tendon constructs cultured in our laboratory (see Calve et al. 2004), is a cylinder 12 mm in length and 1 mm^2 in cross-sectional area, with the orthotropy axis along its length. The initial and boundary conditions have been chosen in order to model a few common mechanical and chemical interventions on engineered tissue. However, we will not attempt detailed descriptions of experiments, choosing to focus instead on results that can be directly related to the models. A more detailed comparison with experiments is forthcoming in a separate communication, and awaits the completion of ongoing experimental studies.

5.1 A numerical demonstration of the formulation

The first example is a numerical demonstration of the formulation with the enhancements to balance laws, kinematics and constitutive relations discussed in Sects. 3.1, 3.2, and 4.2.1–4.2.5. This example uses the upper bound model, and its aim is only to demonstrate that the complexity of the formulation with fluid transport, diffusion-reaction of solute, solid collagen production and mechanics of the composite solid–fluid tissue does not engender numerical instability, as sometimes happens with complex problems.

[10] The mobility tensor reported in Table 1 is an order-of-magnitude estimate recalculated from Han et al. (2000) to correspond to the mobility used in this paper. These authors reported a mean value of 0.927×10^{-14} s, with a range of 0.58×10^{-14}–1.14×10^{-14} s in terms of the mobility used here. Theirs is the mobility parallel to the fiber direction in Rabbit Achilles tendon. Our usage of it is as an isotropic mobility. Using anisotropic mobilities, or different values from the reported range changes the result quantitatively, but not qualitatively.

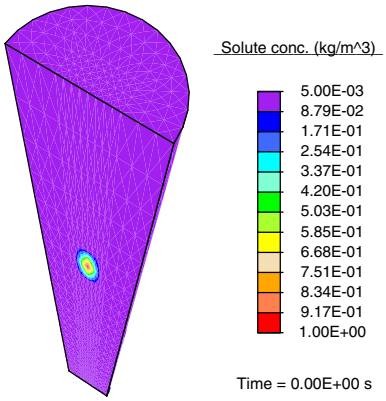

Fig. 3 The solute concentration (kg m^{-3}) initially

The tendon is immersed in a bath. The initial collagen concentration and the initial fluid concentration are both 500 kg m^{-3} at every point in the tendon, and the fluid concentration in the bath is 500 kg m^{-3}. A solute-rich bulb of radius 0.15 mm is introduced (such as by injection) with its centre on the axis of the tendon and situated 3 mm below the upper circular face of the tendon.[11] The initial solute concentration is 0.05 kg m^{-3} at all other points in the tendon, and increases linearly with decreasing radius in this bulb to 1 kg m^{-3} at its centre (see Fig. 3). We use Michaelis–Menten enzyme kinetics (11) to determine the rates of solute consumption and collagen production as a function of solute concentration. Here, the fluid phase does not take part in reactions, and hence $\pi^{\mathrm{f}} = 0$.

The solute undergoes Fickean diffusion from the bulb with graded concentration. Additionally, stress gradient-driven fluid flow is produced by subjecting the tendon to a constrictive radial load, such as would be imposed upon manipulating it with a set of tweezers, as shown in Fig. 4. The maximum strain of 10% in the radial direction is experienced half-way through the height of the tendon. The applied strain in the radial direction decreases linearly with vertical distance from the central plane, and vanishes at the top and bottom surfaces of the tendon.

Figure 5 shows the collagen concentration at an early time, $t = 5 \times 10^{-2}$ s. The contours of solute concentration do not change visibly from Fig. 3 because of the short time involved. The solute in this region has driven the enzyme-kinetics model to result in a small source term for collagen production, and we observe a nominal amount of growth in Fig. 5.

[11] Here, we envision the solute to be a protein playing an essential role in growth by catalysing underlying biochemical reactions. An important example of this is a family of proteins, TGFβ, which is a multifunctional peptide that controls numerous functions of many cell types (Alberts et al. 2002).

Fig. 4 Constrictive load applied to tendon immersed in a bath

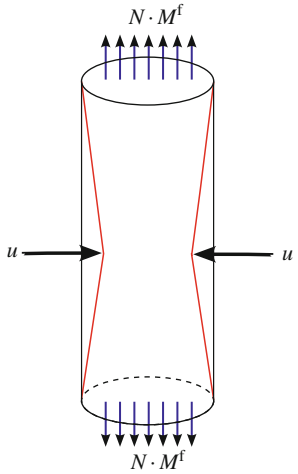

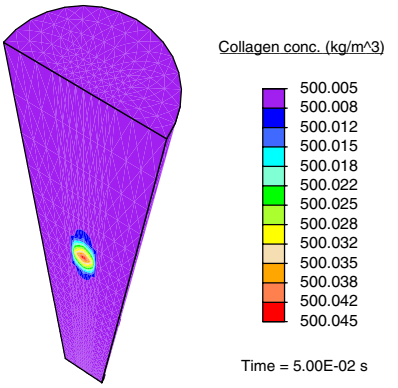

Fig. 5 The collagen concentration (kg m^{-3}) at time $t = 5 \times 10^{-2}$ s

While no numerical instability was observed in this initial and boundary value problem, the drawback to this computation is the exceedingly short physical time of 5×10^{-2} s. This is because convergence of the staggered solution scheme for transport and mechanics is exceedingly slow. It remains slow even when shorn of the complexity of Sects. 3.1, 3.2, and 4.2.1–4.2.5. In order to understand the origins of this slow convergence the formulation was simplified in the following two boundary value problems by suppressing some of the coupled phenomena. This makes it easier to reach slightly longer physical times in the computations.

5.2 Examples exploring the biphasic nature of porous soft tissue

In the calculations that follow, only the fluid and solid collagen are included for the mass transport and mechanics.

5.2.1 The tendon under constriction; upper and lower bound models

In this example, the tendon immersed in a bath is subjected to the same constrictive radial displacement load as in Sect. 5.1.

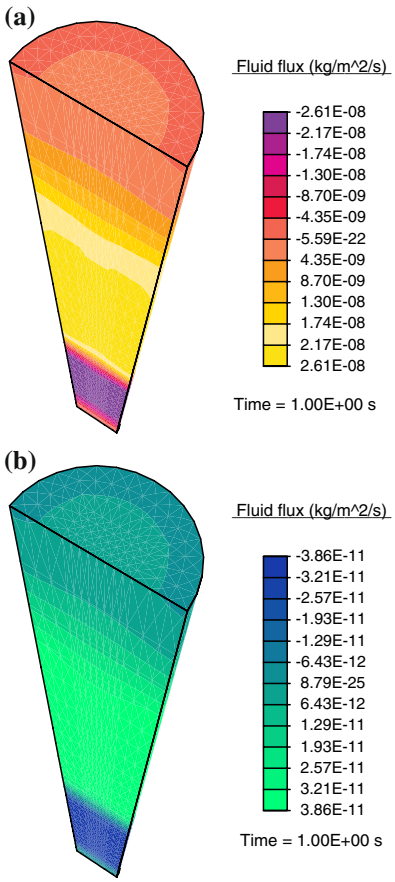

Fig. 6 **a** *Upper bound*, and **b** *lower bound* fluid flux (kg m^{-2} s^{-1}) in the vertical direction at time $t = 1$ s. Attention is drawn to the three orders of magnitude difference between the fluxes from the two models. Note that the contour values of the lower bound model are entirely contained within those of the *upper bound* model

Solute transport-reaction is not considered, and the collagen source, $\Pi^{\mathrm{c}} = 0$. The total duration of the simulation is 10 s, and the radial strain is applied as a displacement boundary condition, increasing linearly from no strain initially to the maximum strain at time $t = 1$ s. As in the first example, the initial collagen concentration and the initial fluid concentration are 500 kg m^{-3} at every point in the tendon, and the fluid concentration is 500 kg m^{-3}. In this case we consider the upper and lower bound models discussed in Sect. 4.3.

For the upper bound model, Fig. 6a shows the fluid flux in the vertical direction at the final stage of the constriction phase of the simulation, i.e., at time $t = 1$ s. The flux values are positive above the central plane, forcing fluid upward, and negative below, forcing fluid downward. This stress gradient-induced fluid flux results in a reference concentration distribution of the fluid that is higher near the top and bottom faces, as seen in Fig. 7.

As a result, these regions would have seen a higher production rate of collagen if the source term Π^{c} had been active, and over time preferential growth would result. As discussed

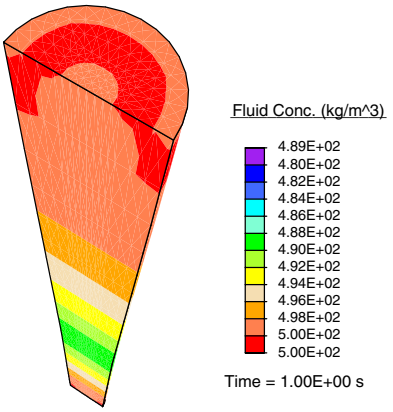

Fig. 7 Reference fluid concentration (kg m^{-3}) at time $t = 1$ s with the *upper bound* model

in Sect. 3.1, the mass transport equations are solved in the current configuration, where physical boundary conditions can be set directly.[12] The values reported in Fig. 7 are pulled back from the current configuration. The current concentrations do not change for this boundary value problem following (19).

The radial strain is held fixed at the value attained at the end of the constriction phase. The time-dependent constriction sets up a pressure wave in the fluid travelling toward the top and bottom faces. As the fluid flows out through these surfaces, the displacement decreases by a measurable amount at the top surface as shown in Fig. 8. The centre of the bottom face of the tendon is fixed in the vertical direction for this computation, and therefore, this surface does not deform vertically.

We turn now to providing numerical evidence in support of the discussion on upper and lower bounds on fluid flux in Sect. 4.3. Figure 6b shows contour values of the vertical flux obtained with the lower bound modelling assumption. The initial and boundary conditions are identical to the computation corresponding to Fig. 6a with the upper bound model, and the solution is also reported at $t = 1$ s, at the end of the constriction phase.

The fluid flux values reported in Fig. 6a, b corresponding to the upper and lower bound models, respectively, differ by about three orders of magnitude. This wide range points to the importance of imposing the appropriate mechanical coupling model between interacting phases. The solution obtained for the same boundary value problem from the two models is strongly influenced by the constitutive relation via the strain- or stress-homogenisation assumption. The bounds that we

[12] The solution of such a problem in the reference configuration using $\rho_0^{\mathrm{f}} = \text{const.}$ as the boundary condition representing the fluid bath yields non-physical results, such as an unbounded flow. This occurs since the imposed strain gradient causes a stress gradient in the fluid that does not decay. The imposed boundary condition on ρ_0^{f} prevents a redistribution of concentration that would have provided an opposing, internal gradient of stress, which in turn would drive the flux to vanish.

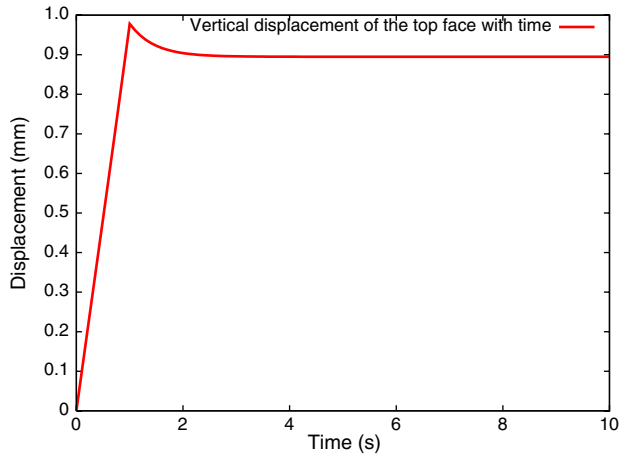

Fig. 8 Retraction of the top face of the tendon after the constriction phase, using the *upper bound* model

have computed for fluid flux values are useful in defining the limits that more precise models will be subject to. In future work, we will describe models for interaction between fluid and solid phases that will replace the upper and lower bound models discussed here and make possible more precise treatment of the mechanical coupling.

This numerical example also points to the fact that a convenient measure of the strength of coupling between the mechanics and mass transport equations is the ratio of the variation in hydrostatic stress of the fluid to that of the solid. In the lower bound case, where the fluid response is defined by Eq. (24), it is instructive to note that this ratio is unity. As a result, it is seen that the lower bound case exhibits significantly weaker coupling than the upper bound case. In the latter, variation in the common deformation gradient, $\delta \boldsymbol{F}$, causes instantaneous variation in $\delta p^{\mathrm{f}} \approx O(\kappa^{\mathrm{f}} \delta \boldsymbol{F} : \boldsymbol{F}^{-\mathrm{T}})$ and in $\frac{1}{3}\delta \mathrm{tr}[\boldsymbol{\sigma}^{\mathrm{c}}] \approx O(\kappa^{\mathrm{c}} \delta \boldsymbol{F} : \boldsymbol{F}^{-\mathrm{T}})$, where κ^{c} is the bulk modulus of the solid. The ratio $\frac{\delta p^{\mathrm{f}}}{\frac{1}{3}\delta \mathrm{tr}[\boldsymbol{\sigma}^{\mathrm{c}}]}$ is, therefore, $\approx O(\kappa^{\mathrm{f}}/\kappa^{\mathrm{c}}) \gg 1$, since $\kappa^{\mathrm{f}} = 1$ GPa and $\kappa^{\mathrm{c}} \approx O(\gamma/\beta) = 222.222$ KPa.

Numerical implications of coupling strength: The strength of coupling between the equations plays a principal role in the rate of convergence of the solution. This is demonstrated in Table 2, where the norm of the finite element force residual for solution of the momentum balance equation, and corresponding CPU times for an Intel® Xeon 3.4 GHz machine are reported for the first eight passes of the staggered scheme for the upper and lower bound models. The table does not report the value of the residual norms arising from the solution of the mass transport equation for the fluid, which occurs after each reported solve of the momentum balance equation. Although the initial residual norms of the momentum balance equation (shown in boldface type) are decreasing linearly in successive passes for both models, the rapid decrease in this quantity in the lower bound case ensures convergence in far fewer iterations than the upper bound model. This confers numerical efficiency upon the lower bound model. In addition to being more physical, as argued at the beginning of Sect. 5.2.2 immediately below, the lower bound model makes it feasible to drive problems to longer, physiologically relevant time-scales through the use of larger time steps.

Table 2 Finite element residual norms for the momentum balance equation and corresponding CPU times in seconds for the first eight passes of upper and lower bound models for a typical time increment, $\Delta t = 0.1$ s

Pass	Upper bound model		Lower bound model	
	Residual	CPU (s)	Residual	CPU (s)
1	$\mathbf{2.138 \times 10^{-02}}$	29.16	$\mathbf{6.761 \times 10^{-04}}$	28.5
	3.093×10^{-04}	55.85	1.075×10^{-04}	55.1
	2.443×10^{-06}	82.37	4.984×10^{-06}	81.8
	2.456×10^{-08}	109.61	1.698×10^{-08}	107.9
	4.697×10^{-14}	135.83	3.401×10^{-13}	134.1
	1.750×10^{-16}	163.18	1.1523×10^{-17}	161.1
2	$\mathbf{5.308 \times 10^{-06}}$	166.79	$\mathbf{5.971 \times 10^{-08}}$	192.5
	4.038×10^{-10}	193.36	4.285×10^{-11}	218.6
	1.440×10^{-14}	220.45	2.673×10^{-15}	246.1
	4.221×10^{-17}	247.04		
3	$\mathbf{5.186 \times 10^{-06}}$	250.62	$\mathbf{2.194 \times 10^{-09}}$	277.3
	3.852×10^{-10}	277.44	2.196×10^{-13}	304.2
	1.369×10^{-14}	304.16	1.096×10^{-17}	331.6
	4.120×10^{-17}	331.47		
4	$\mathbf{5.065 \times 10^{-06}}$	335.16	$\mathbf{8.160 \times 10^{-11}}$	363.2
	3.674×10^{-10}	362.24	7.923×10^{-15}	390.2
	1.300×10^{-14}	388.79		
	4.021×10^{-17}	416.08		
5	$\mathbf{4.948 \times 10^{-06}}$	419.59	$\mathbf{3.078 \times 10^{-12}}$	421.4
	3.503×10^{-10}	446.24	3.042×10^{-16}	448.6
	1.236×10^{-14}	473.20		
	3.924×10^{-17}	500.85		
6	$\mathbf{4.832 \times 10^{-06}}$	504.65	$\mathbf{1.179 \times 10^{-13}}$	479.9
	3.340×10^{-10}	531.28	1.291×10^{-17}	507.0
	1.174×10^{-14}	558.17		
	3.829×10^{-17}	585.27		
7	$\mathbf{4.720 \times 10^{-06}}$	589.01	$\mathbf{4.592 \times 10^{-15}}$	537.8
	3.184×10^{-10}	616.24	5.152×10^{-18}	564.6
	1.116×10^{-14}	643.29		
	3.737×10^{-17}	670.83		
8	$\mathbf{4.609 \times 10^{-06}}$	674.46	$\mathbf{1.816 \times 10^{-16}}$	595.5
	3.034×10^{-10}	701.74	5.040×10^{-18}	622.3
	1.060×10^{-14}	727.74		
	3.646×10^{-17}	755.58		

5.2.2 A problem demonstrating growth and swelling

Motivated mainly by the recognition that the lower bound model for solid–fluid mechanical coupling ensures convergence to a self-consistent solution in just a few passes of the staggered solution scheme, we adopt this version of the coupling for our final problem. On this note, we point out that solution of the individual balances of linear momentum equations for the solid collagenous and fluid phases with the momentum transfer terms [$\boldsymbol{q}^{\mathrm{c}}, \boldsymbol{q}^{\mathrm{f}}$ in (2)] is a statement of momentum balance between them. There is reason to suppose, therefore, that equating the solid collagen and fluid stress, or some component of these tensors as done in the lower bound model, is a reasonable approximation to explicitly solving the balance of linear momentum for each phase, including the momentum transfers. In contrast, equating the deformation gradient of the solid collagen with deformation of the pore spaces as done in the upper bound model subjects the fluid to a stress state also determined by this deformation gradient. This approximation does not correspond to an underlying physical principle comparable to the satisfaction of individual balances of linear momentum for solid collagen and fluid, with momentum transfers. It is, therefore, somewhat less motivated and more questionable. Clearly, a rigorous analysis or numerical comparisons of all three models: upper bound, lower bound and direct solution of individual solid–fluid momentum balances, must be carried out to conclusively demonstrate this. It is a possible topic for a future paper.

In this example, we will demonstrate the mechanical effects of growth due to collagen production, and swelling due to fluid uptake. In the interest of focusing on these aspects, we assume that fibroblasts are available, and that the fluid phase carries the necessary nutrients for collagen production dissolved at a suitable, constant concentration. Collagen production is assumed to be governed by a first-order rate law. Newly produced collagen has proteoglycan molecules bound to it, and they in turn bind water. We model this effect by associating a loss of nutrient-bearing free fluid with collagen production. A fluid sink π^{f} is introduced following first order kinetics,

$$\pi^{\mathrm{f}} = -k^{\mathrm{f}} \left(\rho^{\mathrm{f}} - \rho^{\mathrm{f}}_{\mathrm{ini}} \right), \tag{25}$$

as in Garikipati et al. (2004). Here k^{f} is the reaction rate, taken to be 0.07 s^{-1}, and $\rho^{\mathrm{f}}_{\mathrm{ini}}$ is the initial concentration of fluid. The collagen production is equal to the fluid consumption when written in the reference configuration: $\Pi^{\mathrm{c}} = -\Pi^{\mathrm{f}}$. When $\rho^{\mathrm{f}} > \rho^{\mathrm{f}}_{\mathrm{ini}}$, collagen is produced.

The initial collagen concentration is 500 kg m^{-3} and the fluid concentration is 400 kg m^{-3} at every point in the tendon. When this tendon is subjected to an increase in boundary fluid concentration to 410 kg m^{-3}, i.e., $\rho^{\mathrm{f}}(\boldsymbol{x}, t) = 410$ kg $\mathrm{m}^{-3} \forall \boldsymbol{x} \in \partial\Omega_t$, nutrient-rich fluid is transported into the tissue, due to the pressure difference, induced by the concentration difference, between the fluid in the tendon and at its boundary (fluid stress gradient-driven flux). Thereby, the nutrient concentration is elevated, leading to collagen production, fluid consumption and, eventually, growth due to additional collagen.

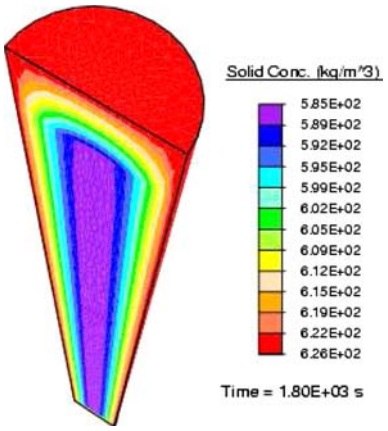

Fig. 9 The collagen concentration after 1,800 s

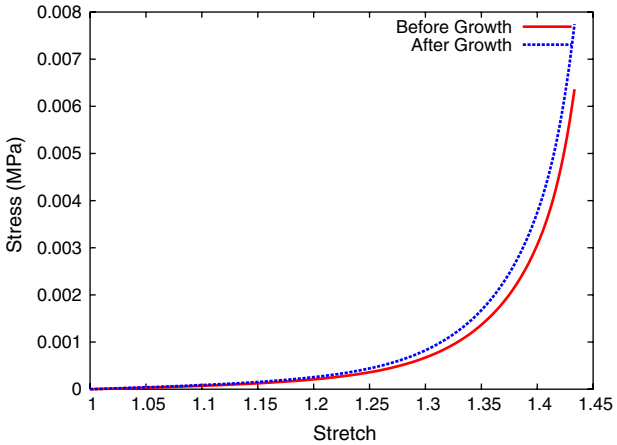

Fig. 10 The stress versus stretch curves before and after growth

After 1,800 s, the tendon shows growth, and the collagen concentration is higher as seen in Fig. 9. On performing a uniaxial tension test on the tendon before and after growth, it is observed (Fig. 10) that the grown tissue is stiffer and stronger due to its higher collagen concentration. While the increase in stiffness is small and probably not discernible in an experiment, this numerical example demonstrates the trend toward greater stiffness. For the example to predict experimentally discernible stiffening would require growth over longer periods with more accurately calibrated models for the collagen source term.

Also note that there is a rapid, fluid transport-dominated swelling of the tendon between 0 and 25 s (Fig. 11). This causes a small volume change of $\approx$1.6%. In this transport-dominated regime the contribution to tendon volume

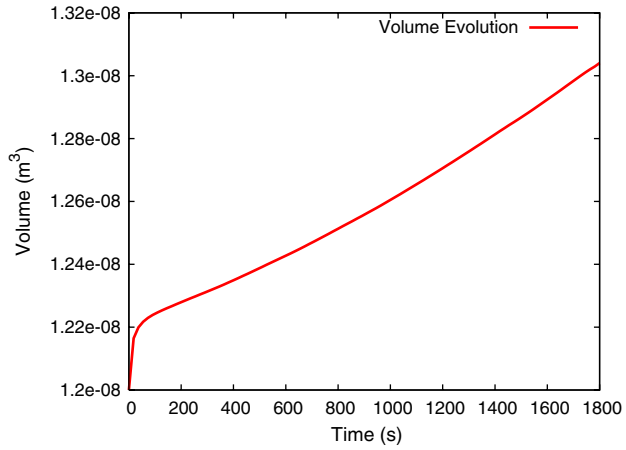

Fig. 11 The volume of the tendon evolving with time. Note the fluid transported-dominated swelling regime until 25 s, followed by the longer reaction-dominated growth stage

change from collagen production is small. However, the fluid-induced swelling saturates, and between 25 and 1,800 s the reaction producing collagen—biological growth—dominates the process, producing a further ≈6.8% volume change. Noting that the range of collagen concentration in Fig. 9 is 585–626 kg m^{-3}, and that (4) gives $\det \boldsymbol{F}^{g^c} = \frac{\rho_0^c}{\rho_{0_{\text{ini}}}^c}$, it is easy to see that the volume change between 25 and 1,800 s is due to collagen production and growth.

6 Closing remarks

In this paper, we have discussed a number of enhancements to our original growth formulation presented in Garikipati et al. (2004). That formulation has served as a platform for posing a very wide range of questions on the physics of growth. Some issues, such as saturation, incompressibility of the fluid species and its influence upon the tissue response, are specific to soft biological tissues. We note, however, that other issues are also applicable to a number of systems with a porous solid, transported fluid and reacting solutes. Included in these are issues of current versus reference configurations for mass transport, swelling, Fickean diffusion, fluid response in compression and tension, cavitation and the strength of solid–fluid coupling.

These issues have been resolved using arguments posed easily in the framework derived in Garikipati et al. (2004). The interactions engendered in the coupled reaction-transport-mechanics system are complex, as borne out by the numerical examples in Sect. 5. The treatment of these issues has led to a formulation more suited to the physics of growing soft tissue, making progress toward our broader goal of applying it to the study of wound healing, pathological hypertrophy and atrophy.

References

Alberts B, Johnson A, Lewis J, Raff M, Roberts K, Walter P (2002) Molecular biology of the cell. Garland Science, Oxford

Ambrosi D, Mollica F (2002) On the mechanics of a growing tumor. Int J Eng Sci 40:1297–1316

Armero F (1999) Formulation and finite element implementation of a multiplicative model of coupled poro-pplasticity at finite strains under fully-saturated conditions. Comp Methods Appl Mech Eng 171:205–241

Bischoff JE, Arruda EM, Grosh K (2002a) A microstructurally based orthotropic hyperelastic constitutive law. J Appl Mech 69:570–579

Bischoff JE, Arruda EM, Grosh K (2002b) Orthotropic elasticity in terms of an arbitrary molecular chain model. J Appl Mech 69:198–201

Brennen CE (1995) Cavitation and bubble dynamics. Oxford University Press, New York

Bromberg S, Dill KA (2002) Molecular driving forces: statistical thermodynamics in chemistry and biology. Garland, Oxford

Brooks A, Hughes T (1982) Streamline upwind/Petrov–Galerkin formulations for convection dominated flows with particular emphasis on the incompressible Navier–Stokes equations. Comp Methods Appl Mech Eng 32:199–259

Calve S, Dennis R, Kosnik P, Baar K, Grosh K, Arruda E (2004) Engineering of functional tendon. Tissue Eng 10:755–761

Cowin SC, Hegedus DH (1976) Bone remodeling I: a theory of adaptive elasticity. J Elast 6:313–325

Epstein M, Maugin GA (2000) Thermomechanics of volumetric growth in uniform bodies. Int J Plast 16:951–978

Fung YC (1993) Biomechanics: mechanical properties of living tissues, 2nd edn. Springer, New York

Garikipati K, Rao VS (2001) Recent advances in models for thermal oxidation of silicon. J Comput Phys 174:138–170

Garikipati K, Arruda EM, Grosh K, Narayanan H, Calve S (2004) A continuum treatment of growth in biological tissue: mass transport coupled with mechanics. J Mech Phys Solids 52:1595–1625

Garikipati K, Olberding JE, Narayanan H, Arruda EM, Grosh K, Calve S (2006) Biological remodelling: stationary energy, configurational change, internal variables and dissipation. J Mech Phys Solids 57:1493–1515

Han S, Gemmell SJ, Helmer KG, Grigg P, Wellen JW, Hoffman AH, Sotak CH (2000) Changes in ADC caused by tensile loading of rabbit achilles tendon: evidence for water transport. J Magn Reson 144:217–227

Hughes T, Franca L, Mallet M (1987) A new finite element formulation for computational fluid dynamics: VII. Convergence analysis of the generalized SUPG formulation for linear time-dependent multidimensional advective–diffusive systems. Comp Methods Appl Mech Eng 63(1):97–112

Humphrey JD, Rajagopal (2002) A constrained mixture model for growth and remodeling of soft tissues. Math Methods Mod Appl Sci 12(3):407–430

Klisch SM, van Dyke TJ, Hoger A (2001) A theory of volumetric growth for compressible elastic biological materials. Math Mech Solids 6:551–575

Kratky O, Porod G (1949) Röntgenuntersuchungen gelöster Fadenmoleküle. Recl Trav Chim 68:1106–1122

Kuhl E, Garikipati K, Arruda E, Grosh K (2005) Remodeling of biological tissue: mechanically induced reorientation of a transversely isotropic chain network. J Mech Phys Solids (UK) 53(7):1552–1573

Lee EH (1969) Elastic–plastic deformation at finite strains. J Appl Mech 36:1–6

Milton GW (2002) Theory of composites. Cambridge University Press, London

Nordin M, Lorenz T, Campello M (2001) Biomechanics of tendons and ligaments. In: Nordin M, Frankel VH (eds) Basic biomechanics of the musculoskeletal system. Lippincott Williams and Wilkins, New York, pp 102–125

Rao VS, Hughes TJR, Garikipati K (2000) On modelling thermal oxidation of silicon ii: Numerical aspects. Int J Numer Methods Eng 47(1/3):359–378

Rodriguez EK, Hoger A, McCullough AD (1994) Stress-dependent finite growth in soft elastic tissues. J Biomech 27:455–467

Sengers BG, Oomens CWJ, Baaijens FPT (2004) An integrated finite-element approach to mechanics, transport and biosynthesis in tissue engineering. J BioMech Eng 126:82–91

Simo JC, Taylor RL, Pister KS (1985) Variational and projection methods for the volume constraint in finite deformation elasto-plasticity. Comp Methods Appl Mech Eng 51:177–208

Taber LA, Humphrey JD (2001) Stress-modulated growth, residual stress and vascular heterogeneity. J BioMech Eng 123:528–535

Taylor RL (1999) FEAP—a finite element analysis program. University of California at Berkeley, Berkeley

Tezduyar T, Sathe S (2003) Stabilization parameters in SUPG and PSPG formulations. J Comput Appl Mech 4:71–88

Truesdell C, Noll W (1965) The non-linear field theories (Handbuch der Physik, band III). Springer, Berlin